Editors' Suggestion | Featured in Physics

Precision Metrology Meets Cosmology: Improved Constraints on Ultralight Dark Matter from Atom-Cavity Frequency Comparisons

Colin J. Kennedy,[1] Eric Oelker,[1,*] John M. Robinson,[1] Tobias Bothwell,[1] Dhruv Kedar,[1] William R. Milner,[1] G. Edward Marti,[1,2] Andrei Derevianko,[3] and Jun Ye[1]

[1]*JILA, National Institute of Standards and Technology and University of Colorado, Boulder, Colorado 80309-0440, USA*

[2]*Department of Molecular and Cellular Physiology, Stanford University, Stanford, California 94305, United States*

[3]*Department of Physics, University of Nevada, Reno, Nevada 89557, USA*

(Received 19 August 2020; accepted 7 October 2020; published 12 November 2020)

We conduct frequency comparisons between a state-of-the-art strontium optical lattice clock, a cryogenic crystalline silicon cavity, and a hydrogen maser to set new bounds on the coupling of ultralight dark matter to standard model particles and fields in the mass range of $10^{-16} - 10^{-21}$ eV. The key advantage of this two-part ratio comparison is the differential sensitivity to time variation of both the fine-structure constant and the electron mass, achieving a substantially improved limit on the moduli of ultralight dark matter, particularly at higher masses than typical atomic spectroscopic results. Furthermore, we demonstrate an extension of the search range to even higher masses by use of dynamical decoupling techniques. These results highlight the importance of using the best-performing atomic clocks for fundamental physics applications, as all-optical timescales are increasingly integrated with, and will eventually supplant, existing microwave timescales.

DOI: 10.1103/PhysRevLett.125.201302

It is widely accepted that dark matter makes up the majority of the matter in the observable Universe [1,2]. While its composition remains a mystery, its presence is manifest through gravitational effects on galactic and cosmological scales [3–5]. Many efforts on direct detection with laboratory experiments target weakly interacting massive particles with masses in the 100 GeV range as suitable candidate particles arise naturally in popular extensions to the standard model [6–9]. Axions are another class of particle that has garnered interest both in solving the strong *CP* problem and as a dark matter candidate [10–12]. The pseudoscalar coupling of axions to matter dictates searches for odd parity signals such as permanent electric dipole moments of the neutron or electron [13,14], conversion of axions to photons in a strong magnetic field [15,16], nuclear recoils [17], and axions coupling to electron spin flips [18–21].

Another active consideration focuses on dilatonic dark matter particles arising from extra dimensions whose masses span many orders of magnitude below 1 eV down to 10^{-22} eV, where the particle's wavelength is comparable to the size of dwarf galaxies. In this low-energy regime, the conditions that the dark matter with large de Broglie wavelengths is gravitationally bound to galaxies imply that these particles have large occupation numbers per mode and, consequently, form a highly coherent bosonic object behaving locally like a classical field [22]. While astrophysical consequences of such an ultralight field produce various constraints [23–26], including potential constraints from the test of black hole superradiance [27–30], development of new laboratory probes for scalar fields can provide natural solutions to some astrophysical problems such as small-scale structure in typical cold dark matter models [31]. Specifically, ultralight bosonic dark matter with couplings to normal matter is predicted to generate highly coherent oscillations in the fine-structure constant as well as electron and quark masses [32–34]. Additionally, assuming that the dark matter contains self-interaction, it may form clumps that can manifest as transient changes in these constants [35–39].

Using atomic clocks as probes of ultralight dark matter has garnered strong interest due to their inherent sensitivity to fundamental constants and the rapid advance in the clock performance over the past decade. These systems provide a promising route to advance the search frontier for ultralight dark matter particles given a wealth of historical data from global timescale systems [38,40–43], including GPS [37], and a host of recent proposals for enhancing the sensitivity of optical lattice clocks for dark matter searches [44,45].

In this Letter, we demonstrate significantly improved bounds on the coupling of ultralight dark matter to the fine-structure constant (α) and electron mass (m_e). Central to this important advance is the state-of-the-art stability of our 21 cm crystalline silicon optical cavity at 124 K [46–48] and measuring its frequency with both a Sr optical lattice clock with an estimated accuracy of 2.0×10^{-18} [49] and a hydrogen maser [50]. Figure 1(a) shows the cavity resonance frequency in atomic units, $f_c \propto \alpha m_e c^2$, and its

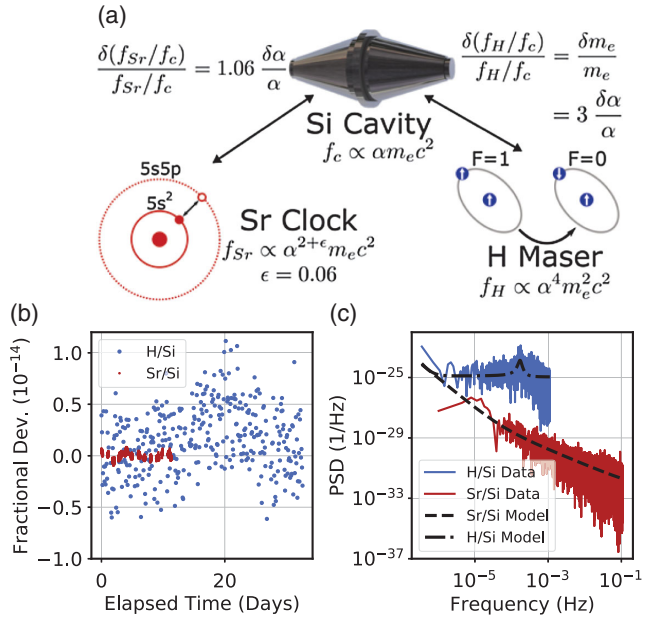

FIG. 1. Atom-cavity frequency comparisons. (a) Schematic depiction of the three frequencies that compose the ratios for this dark matter search. Fractional fluctuations of these ratios are sensitive to fractional fluctuations of fundamental quantities via the inscribed equations. (b) Time-domain signal of the 12-day comparison for the f_{Sr}/f_c ratio (red) and the 33-day comparison of f_{H}/f_c (blue). For visual clarity, f_{H}/f_c has been decimated by a factor of 720. (c) Frequency-domain signal derived from (b) using the Lomb-Scargle technique to estimate the PSD. Data for f_{Sr}/f_c have a bin width of 3.4×10^{-6} Hz and for f_{H}/f_c have a bin width of 3.7×10^{-7} Hz. Black lines indicate the noise model for f_{Sr}/f_c (dashed) and f_{H}/f_c (dot-dashed) ratios.

dependence on α and m_e, both of which are directly traceable to the Bohr radius, as the cavity spacer length is proportional to the silicon crystal lattice constant. The frequency of a resonant mode of the cavity is compared to atomic standards in both the optical and microwave domains, forming the dimensionless frequency ratios shown in Fig. 1(a). These atomic standards have different dependencies on α and m_e, making these dimensionless ratios powerful sensors for potential physics beyond the standard model. For the optical ratio, the ^{87}Sr clock transition frequency depends primarily on the Rydberg energy $\frac{1}{2}\alpha^{2+\epsilon} m_e c^2$ via the electron interaction energy difference between $5s^2$ and $5s5p$ clock states—with a small $\epsilon = 0.06$ correction for relativistic effects [51]. For the microwave ratio, the ^{1}H hyperfine transition frequency depends on the magnetic interaction of the electron and nuclear spins, $f_{\mathrm{H}} \propto \alpha^4 m_e^2 c^2$, leading to a different dependence on α and m_e [52]. While not discussed in detail here, f_{H}/f_c has additional sensitivity to the quark masses, the results of which are given in Ref. [53].

Arising from this differential sensitivity to fundamental constants, precise determination of the fluctuations of both f_{H}/f_c and f_{Sr}/f_c provides a direct correspondence with potential fluctuations in the apparent values of fundamental constants. These relative fluctuations can subsequently be used to connect cosmological models of dark matter to atomic physics experiments via various hypotheses of how the standard model is coupled to dark matter. To make this connection, we consider the Lagrangian coupling terms (in natural units $\hbar = c = 1$) between dark matter, ϕ, and standard model particles and fields [32]:

$$\mathcal{L}_\phi = \kappa\phi\left(\frac{d_e}{4}F_{\mu\nu}F^{\mu\nu} - d_{m_e} m_e \overline{\psi}_e \psi_e\right). \tag{1}$$

The first term describes the coupling of ϕ to α via the electromagnetic Faraday tensor $F_{\mu\nu}$, with the electromagnetic gauge modulus d_e, and $\kappa = \sqrt{4\pi G_N}$ with Newton's constant G_N. The second term describes the coupling of ϕ to m_e with the modulus d_{m_e} and the electron field ψ_e. In this model, $\mathcal{L}_\phi$ produces an apparent periodic change in α or m_e, with the modulus d_e or d_{m_e}, respectively. This manifests in a laboratory experiment as periodic oscillations of dimensionless frequency ratios at the Compton frequency (f_ϕ), which can be subsequently used to set bounds on both d_e and d_{m_e} [53].

The data composing the two dimensionless frequency ratios are shown in Fig. 1(b). To begin, we consider a potential periodic signal that is observed over a duration of T_{max}, compared to the dark matter field's coherence time τ_c. For $T_{\mathrm{max}} < \tau_c$, the phase is preserved throughout the observation run, so we expect the signal-to-noise ratio to improve as more data are collected. The f_{Sr}/f_c data consist of 12 consecutive comparison days with a total uptime of 30% resulting in a dataset that is 978 041 s long. The f_{H}/f_c data span 33 days and have a total uptime of 94% resulting in a 2 826 942 s long record. The highest frequency and mass bins for the Sr-Si dataset are at 125 mHz, corresponding to a time period of 8 s, or a maximum of 1.2×10^5 oscillations over the course of comparison, whereas the expected virial velocity broadening of dark matter expects coherence times up to 10^6 oscillations, $\tau_c = (f_\phi v_{\mathrm{virial}}^2/c^2)^{-1}$ [32]. Consequently, the results of this comparison are interpreted in the limit of $T_{\mathrm{max}} < \tau_c$.

The power-spectral density (PSD) of the data is shown in Fig. 1(c). The f_{Sr}/f_c model, shown overlaid in black dashed lines, is derived from previous work adding in a white frequency noise term accounting for the Dick effect [48]. The f_{H}/f_c model, shown in dash-dotted lines, is derived from the cavity model in addition to a white frequency noise term for the maser. A resonance around 0.1 mHz accounts for the noise of the microwave link between the maser location at NIST and the cavity and optical frequency comb at JILA [53]. The PSD can be converted into a power spectrum using the bin width and, subsequently, a bound on the coupling of dark matter to standard model fields after accounting for the contribution of the realistic laser noise in each frequency bin.

Complications arise from the existence of time gaps in the data and the flicker frequency and random walk noise contributions in the frequency record. As a result, traditional methods for computing the power spectrum of the data are not accurate estimators of the true power spectrum. To handle the gapped data, we use a Lomb-Scargle periodogram implemented using publicly available software from the astropy PYTHON library [54,55]. In the limit of a continuous dataset without gaps, the Lomb-Scargle periodogram is equivalent to traditional techniques for evaluating the power spectrum even in the presence of correlated noise [53]. For f_{Sr}/f_c, the periodogram is evaluated at frequencies ranging from the sampling frequency of 125 mHz to the frequency corresponding to one oscillation over the total duration of the dataset. The number of bins this frequency range is subdivided into is given by one-half of the total number of measurements taken during the observation period. Data for f_{H}/f_c are longer in duration, have significantly fewer gaps, and are dominated by white noise, but nonetheless the power spectrum is evaluated with the same procedure as f_{Sr}/f_c. Because of the worse short-term stability of f_{H}/f_c and the presence of significant microwave link noise at high frequencies [50], data for the maser are plotted only for frequencies below 1 mHz [53].

Given this technique for estimating the power spectrum of the gapped data, we next consider the amount of power observed in each frequency bin and the likelihood of observing that signal given the known laser noise model in the two-part frequency comparison. To accomplish this, the known model for each ratio is used to simulate the expected noise on a continuous dataset. These data are then gapped in accordance with the timestamps of the real experiment, and the Lomb-Scargle algorithm is used to estimate the power spectrum of the simulated data. This procedure is repeated 1000 times to generate a probability distribution of expected power for each frequency bin given the laser model and the existing gaps in the data [53]. For each bin, the 95% confidence limit can thus be determined by numerical integration of this probability distribution. This procedure is especially important for low-frequency bins corresponding to timescales longer than an individual day's data, as the presence of gaps in the dataset reduces the sensitivity of the search to oscillations of specific frequencies. This is seen most prominently at masses ranging from 4×10^{-20} to 1×10^{-18} eV arising from the diurnal pattern of data collection, with more discussion on data gaps provided in Ref. [53].

The amplitude spectrum is then derived from the observed and expected power spectrum, and the direct relation between the fractional amplitude in each bin and limits on d_e and d_{m_e} is determined. To provide a rigorous confirmation of all limits derived in this Letter, we inject a periodic signal into the analysis pipeline with a known frequency and amplitude to demonstrate that our approach provides the correct sensitivity limit for detection [53]. In the analysis, we subtract the overall linear drift of the laser cavity or the hydrogen maser. For this reason, we do not consider any frequencies below the inverse duration of the dataset. With artificial signal injection, the impact of this subtraction underestimates the lowest frequency bin only by a factor of 2.3 and is corrected accordingly.

Figure 2(a) shows the limits on d_e derived from both f_{Sr}/f_c (red) and f_{H}/f_c (blue). These results surpass previous limits, and particularly at higher masses, on d_e set by atomic spectroscopy (black lines) of Dy [56], Rb and Cs atomic clocks [57], and an optical clock network [38]. Figure 2(b) shows the limits on d_{m_e} derived from f_{H}/f_c.

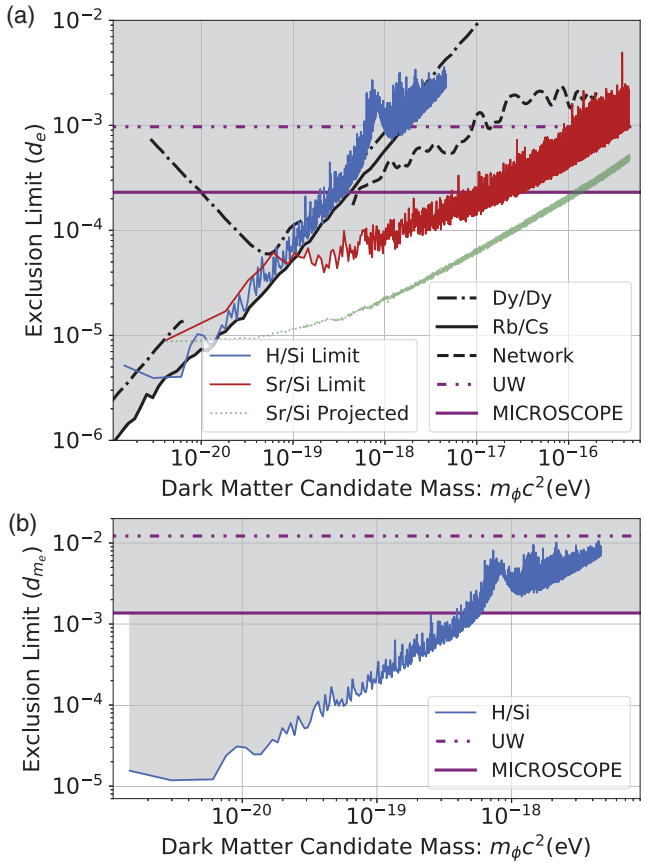

FIG. 2. Dilatonic dark matter exclusion plot. (a) 95% confidence limits placed on the electromagnetic gauge modulus d_e, showing the improved limits set by f_{Sr}/f_c (red) and f_{H}/f_c (blue) ratios in the mass range above 1×10^{-19} eV. The maximum projected sensitivity for a search of the same 11-day duration without data gaps is included (light green), highlighting the potential of this technique. Limits derived from previous spectroscopic searches (black lines) [38,56,57] and equivalence principle tests (purple lines) [58,59] are included. (b) Demonstration of a significantly improved limit on the electron mass modulus (d_{m_e}) derived from the f_{H}/f_c (blue) ratio. Limits from equivalence principle tests (purple lines) [58,59] are included. Shaded regions in both (a) and (b) are excluded at the 95% confidence level given the observed signal and noise models.

As recently highlighted in Ref. [60], interferences of different amplitudes that are thought to compose the local thermal state of the dark matter field create a distribution of possible field amplitudes ϕ, observed locally. As the apparent variation of constants comes from ϕ acting on α or m_e, the limit for the moduli d_e and d_{m_e} thus depends on the value of ϕ experienced locally. When $T_{\max} < \tau_c$, the experiment is sampling from this distribution once, and the nondeterministic amplitude affects the exclusion region of d_e and d_{m_e}. This effect is captured in Fig. 2 by a uniform rescaling of all spectroscopic limits previously published by a factor of 3.0 in accordance with the 95% limit of this distribution.

At the same time, limits on d_e and d_{m_e} are also set by equivalence principle tests [58,59,61,62] with the most stringent limits to date coming from measurements of differential accelerations of macroscopic masses [58,59], plotted in Fig. 2 (purple lines). These limits are not affected by the stochastic amplitude of ϕ, because the coupling to dark matter in this case arises through a virtual exchange of the ultralight dark matter particle that mediates a Yukawa potential. Therefore, these searches are not affected by the rescaling as in spectroscopic searches.

Figure 2 shows the limits established by both f_{Sr}/f_c and f_{H}/f_c on d_e and d_{m_e} at the 95% confidence level. For d_e, we set a new bound at a range of masses from 1×10^{-17} to 1×10^{-19} eV and improve upon the limits coming from atomic spectroscopy (black lines) from 4.5×10^{-16} down to 1×10^{-19} eV, improving the limit by a factor of 5 in certain mass ranges. One prominent, high-Q peak at 3.83×10^{-16} is identified as arising from magnetic field noise which is imperfectly rejected by the atomic servo. For d_{m_e}, f_{H}/f_c are the only data with sensitivity, and here we improve the limit by up to a factor of 100 between 2×10^{-19} and 2×10^{-21} eV. This disfavors d_{m_e} at the level of $\sim 4 \times 10^{-5}$ for the lowest masses and can easily be improved and extended to lower candidate masses when longer datasets are collected. For comparison, Ref. [63] discusses natural values of both d_e and d_{m_e} and shows that the current limits on d_{m_e} are $\sim 10^6$ above natural values for this parameter. In total, the data do not support a signal consistent with coupling of dark matter to standard model particles and fields subject to the constraints of the known cavity and maser noise models.

To expand the sensitivity of the search to a higher mass range beyond 10^{-16} eV [52,64], we demonstrate a technique of dynamical decoupling during the operation of the Sr lattice clock [65–68]. Figure 3(a) details the time sequence for this search, consisting of interleaved Ramsey and echo sequences used for clock operation and high-frequency sampling, respectively. The clock sequence locks the laser to the atomic resonance and enables near-continuous probing of the high-frequency noise for many consecutive hours. Figure 3(b) shows the resulting measurements of the excitation fraction for the

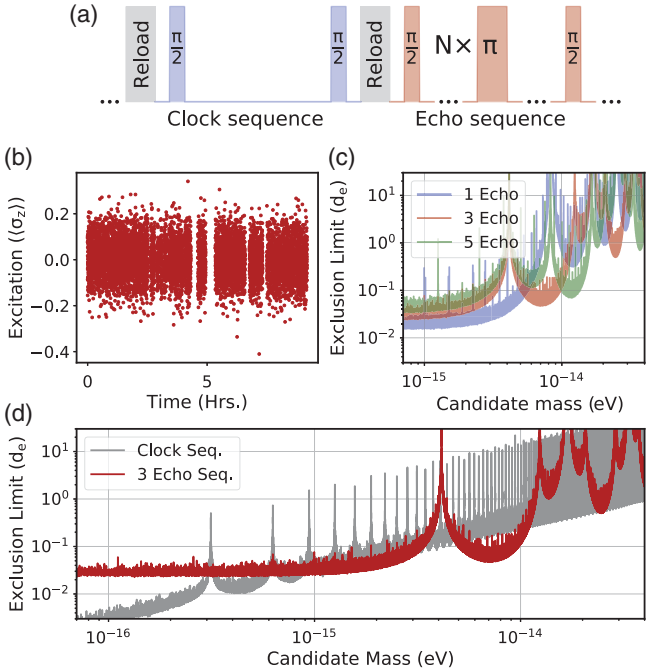

FIG. 3. High-frequency search with dynamical decoupling. (a) Experimental sequence to interleave clock and spin-echo pulses. The dark time for both sequences is 1 s, with the number of echo pulses $N = 1$, 3, and 5. (b) Time-domain signal for the three-pulse sequence over a single day of data collection, or 33 043 s. (c) Limits derived from each of the three pulse sequences demonstrating the flexibility in tailoring the sensitivity function for targeted searches. (d) Comparison of the limit derived from interpolating the low-frequency data of the clock sequence to higher frequencies (gray) compared to the dynamical decoupling sequence for $N = 3$ (red) showing clear advantage for frequencies above the Nyquist frequency and the customized sensitivity for specific mass regions.

case of a three-echo pulse sequence ($N = 3$) converted into units of $\langle \sigma_z \rangle$, in the basis of $\{|g\rangle, |e\rangle\}$ ground- and excited-clock states, respectively. For a highly coherent oscillation, extending the total observation time up to the expected coherence time of the dark matter field increases the search sensitivity. Here, each echo sequence had a limited data length and, thus, the ultimate limit that can be set by this technique. With longer observation times, an expected improvement of ~ 100 is attainable, thereby making such a search compelling.

For the high-frequency search, we conduct three separate experiments varying the number of echo pulses between $N = 1$, 3, and 5. For all pulse sequences, including the clock sequence, we use an evolution time of 1 s between the initial and final $\pi/2$ pulses with π pulses of 28 ms in duration. Each search produces two signals for f_{Sr}/f_c, one at low frequencies coming from the control and error signals of the clock sequence and another at high frequencies coming from the echo sequence. Each is converted to a limit at masses above the sampling frequency of the clock

using the analysis outlined in Ref. [53]. Figure 3(c) shows the resulting limits for each of the three dynamical decoupling pulse sequences. The ability to tailor the search range and sensitivity is apparent. Additionally, many sharp resonances appear in the spectrum which are found to be consistent with the known laser model by comparison with simulation.

Figure 3(d) demonstrates the advantage of dynamical decoupling when compared to an extension of a low-frequency search to higher frequency. First, the ability to tune the point of maximal sensitivity is evident by the lower limit achieved at masses around 7×10^{-15} eV. Second, the limit derived from dynamical decoupling does not suffer from reduced sensitivity at every multiple of the Nyquist frequency as is apparent in the limit derived from the clock sequence. Note that the exclusion limits shown in Figs. 3(c) and 3(d) have been corrected for the assumption of a stochastic dark matter field amplitude as in Fig. 2.

The new limits demonstrated in this work highlight how the search for new physics is enabled directly by the higher degree of frequency stability demonstrated by cryogenic Si cavities [48] as well as the improved accuracy, stability, and long-term reliability of the optical lattice clock [49]. This improved stability allows observing the fractional variation of the frequency ratios in this three-element network with a higher degree of precision than previously possible. This also shows that, as the stability of optical cavities and the precision and total uptime of optical clocks improve over time, each advance enables the reexamination of this result with progressively higher resolution. Integrated with a microwave timescale, future timekeeping systems will be able to extend the discovery reach of these searches for dark-matter-induced variation of fundamental constants. Indeed, the data presented here are a subset of that used to demonstrate an all-optical timescale with a record low timing error over one month of operation [50]. As ultra-stable laser technologies and laser cooling techniques advance to include atomic species with highly relativistic clock transitions in neutral atoms, ions, highly charged ions, and nuclei, the resolution with which these effects can be resolved is expected to advance greatly.

We thank T. Fortier, J. A. Sherman, and H. Leopardi for the maser connection, D. Matei, T. Legero, U. Sterr, and F. Riehle for the collaboration on silicon cavities, and S. Campbell, R. Hutson, A. Goban, S. Kolkowitz, Y. Stadnik, K. Van Tilburg, S. Dimopoulos, and M. Arvanitaki for useful discussions. We acknowledge funding support from NIST, Defense Advanced Research Projects Agency, and National Science Foundation QLCI Award No. OMA - 2016244, NSF Phys-1734006, and PHY-1912465.

*Present address: School of Physics and Astronomy, SUPA, University of Glasgow, Glasgow G12 8QQ, United Kingdom.

[1] D. N. Schramm and M. S. Turner, Rev. Mod. Phys. **70**, 303 (1998).
[2] G. Bertone, *Particle Dark Matter: Observations, Models and Searches* (Cambridge University Press, Cambridge, England, 2010).
[3] J. Bovy and S. Tremaine, Astrophys. J. **756**, 89 (2012).
[4] D. Clowe, M. Bradač, A. H. Gonzalez, M. Markevitch, S. W. Randall, C. Jones, and D. Zaritsky, Astrophys. J. **648**, L109 (2006).
[5] N. Aghanim *et al.*, Astron. Astrophys. **641**, A6 (2020).
[6] E. Aprile, J. Aalbers, F. Agostini, M. Alfonsi, L. Althueser, F. D. Amaro *et al.* (XENON Collaboration), Phys. Rev. Lett. **121**, 111302 (2018).
[7] M. Ackermann, A. Albert, B. Anderson, W. B. Atwood, L. Baldini, G. Barbiellini *et al.* (Fermi-LAT Collaboration), Phys. Rev. Lett. **115**, 231301 (2015).
[8] X. Cui, A. Abdukerim, W. Chen, X. Chen, Y. Chen, B. Dong, D. Fang, C. Fu, K. Giboni, F. Giuliani *et al.*, Phys. Rev. Lett. **119**, 181302 (2017).
[9] M. Aaboud, G. Aad, B. Abbott, B. Abeloos, S. Abidi, O. AbouZeid, N. L. Abraham, H. Abramowicz, H. Abreu, R. Abreu *et al.*, J. High Energy Phys. (2018) 126.
[10] J. Preskill, M. B. Wise, and F. Wilczek, Phys. Lett. **120B**, 127 (1983).
[11] L. F. Abbott and P. Sikivie, Phys. Lett. **120B**, 133 (1983).
[12] M. Dine and W. Fischler, Phys. Lett. **120B**, 137 (1983).
[13] C. Abel, N. J. Ayres, G. Ban, G. Bison, K. Bodek, V. Bondar, M. Daum, M. Fairbairn, V. V. Flambaum, P. Geltenbort *et al.*, Phys. Rev. X **7**, 041034 (2017).
[14] T. S. Roussy, D. A. Palken, W. B. Cairncross, B. M. Brubaker, D. N. Gresh, M. Grau, K. C. Cossel, K. Boon Ng, Y. Shagam, Y. Zhou, V. V. Flambaum, K. W. Lehnert, J. Ye, and E. A. Cornell, arXiv:2006.15787.
[15] N. Du, N. Force, R. Khatiwada, E. Lentz, R. Ottens, L. Rosenberg, G. Rybka, G. Carosi, N. Woollett, D. Bowring *et al.* (ADMX Collaboration), Phys. Rev. Lett. **120**, 151301 (2018).
[16] L. Zhong, S. Al Kenany, K. M. Backes, B. M. Brubaker, S. B. Cahn, G. Carosi, Y. V. Gurevich, W. F. Kindel, S. K. Lamoreaux, K. W. Lehnert *et al.*, Phys. Rev. D **97**, 092001 (2018).
[17] E. Aprile, J. Aalbers, F. Agostini, M. Alfonsi, L. Althueser, F. Amaro, V. Antochi, E. Angelino, J. Angevaare, F. Arneodo *et al.* (XENON Collaboration), Phys. Rev. D **102**, 072004 (2020).
[18] A. Garcon, J. W. Blanchard, G. P. Centers, N. L. Figueroa, P. W. Graham, D. F. J. Kimball, S. Rajendran, A. O. Sushkov, Y. V. Stadnik, A. Wickenbrock *et al.*, Sci. Adv. **5**, eaax4539 (2019).
[19] T. Wu, J. W. Blanchard, G. P. Centers, N. L. Figueroa, A. Garcon, P. W. Graham, D. F. Jackson Kimball, S. Rajendran, Y. V. Stadnik, A. O. Sushkov, A. Wickenbrock, and D. Budker, Phys. Rev. Lett. **122**, 191302 (2019).
[20] W. A. Terrano, E. G. Adelberger, C. A. Hagedorn, and B. R. Heckel, Phys. Rev. Lett. **122**, 231301 (2019).
[21] N. Crescini, D. Alesini, C. Braggio, G. Carugno, D. D'Agostino, D. Di Gioacchino, P. Falferi, U. Gambardella, C. Gatti, G. Iannone *et al.*, Phys. Rev. Lett. **124**, 171801 (2020).
[22] M. S. Safronova, D. Budker, D. DeMille, D. F. J. Kimball, A. Derevianko, and C. W. Clark, Rev. Mod. Phys. **90**, 025008 (2018).

[23] D. J. E. Marsh and J. C. Niemeyer, Phys. Rev. Lett. **123**, 051103 (2019).
[24] N. K. Porayko, X. Zhu, Y. Levin, L. Hui, G. Hobbs, A. Grudskaya, K. Postnov, M. Bailes, N. D. R. Bhat, W. Coles *et al.* (PPTA Collaboration), Phys. Rev. D **98**, 102002 (2018).
[25] V. Iršič, M. Viel, M. G. Haehnelt, J. S. Bolton, and G. D. Becker, Phys. Rev. Lett. **119**, 031302 (2017).
[26] L. Visinelli and S. Vagnozzi, Phys. Rev. D **99**, 063517 (2019).
[27] A. Arvanitaki, M. Baryakhtar, and X. Huang, Phys. Rev. D **91**, 084011 (2015).
[28] M. J. Stott and D. J. E. Marsh, Phys. Rev. D **98**, 083006 (2018).
[29] V. Cardoso, Ó. J. Dias, G. S. Hartnett, M. Middleton, P. Pani, and J. E. Santos, J. Cosmol. Astropart. Phys. 03 (2018) 043.
[30] H. Davoudiasl and P. B. Denton, Phys. Rev. Lett. **123**, 021102 (2019).
[31] W. Hu, R. Barkana, and A. Gruzinov, Phys. Rev. Lett. **85**, 1158 (2000).
[32] A. Arvanitaki, J. Huang, and K. Van Tilburg, Phys. Rev. D **91**, 015015 (2015).
[33] Y. V. Stadnik and V. V. Flambaum, Phys. Rev. Lett. **114**, 161301 (2015).
[34] Y. V. Stadnik and V. V. Flambaum, Phys. Rev. Lett. **115**, 201301 (2015).
[35] A. Derevianko and M. Pospelov, Nat. Phys. **10**, 933 (2014).
[36] P. Wcisło, P. Morzyński, M. Bober, A. Cygan, D. Lisak, R. Ciuryło, and M. Zawada, Nat. Astron. **1**, 0009 (2017).
[37] B. M. Roberts, G. Blewitt, C. Dailey, M. Murphy, M. Pospelov, A. Rollings, J. Sherman, W. Williams, and A. Derevianko, Nat. Commun. **8**, 1195 (2017).
[38] P. Wcisło, P. Ablewski, K. Beloy, S. Bilicki, M. Bober, R. Brown, R. Fasano, R. Ciuryło, H. Hachisu, T. Ido *et al.*, Sci. Adv. **4**, eaau4869 (2018).
[39] Y. V. Stadnik, arXiv:2006.00185.
[40] N. Huntemann, B. Lipphardt, C. Tamm, V. Gerginov, S. Weyers, and E. Peik, Phys. Rev. Lett. **113**, 210802 (2014).
[41] R. M. Godun, P. B. R. Nisbet-Jones, J. M. Jones, S. A. King, L. A. M. Johnson, H. S. Margolis, K. Szymaniec, S. N. Lea, K. Bongs, and P. Gill, Phys. Rev. Lett. **113**, 210801 (2014).
[42] S. Blatt, A. D. Ludlow, G. K. Campbell, J. W. Thomsen, T. Zelevinsky, M. M. Boyd, J. Ye, X. Baillard, M. Fouché, R. Le Targat, A. Brusch, P. Lemonde, M. Takamoto, F.-L. Hong, H. Katori, and V. V. Flambaum, Phys. Rev. Lett. **100**, 140801 (2008).
[43] T. Rosenband, D. Hume, P. Schmidt, C.-W. Chou, A. Brusch, L. Lorini, W. Oskay, R. E. Drullinger, T. M. Fortier, J. Stalnaker *et al.*, Science **319**, 1808 (2008).
[44] J. C. Berengut, V. A. Dzuba, and V. V. Flambaum, Phys. Rev. Lett. **105**, 120801 (2010).
[45] M. S. Safronova, S. G. Porsev, C. Sanner, and J. Ye, Phys. Rev. Lett. **120**, 173001 (2018).
[46] T. Kessler, C. Hagemann, C. Grebing, T. Legero, U. Sterr, F. Riehle, M. Martin, L. Chen, and J. Ye, Nat. Photonics **6**, 687 (2012).
[47] D. G. Matei, T. Legero, S. Häfner, C. Grebing, R. Weyrich, W. Zhang, L. Sonderhouse, J. M. Robinson, J. Ye, F. Riehle, and U. Sterr, Phys. Rev. Lett. **118**, 263202 (2017).
[48] E. Oelker, R. Hutson, C. Kennedy, L. Sonderhouse, T. Bothwell, A. Goban, D. Kedar, C. Sanner, J. Robinson, G. Marti *et al.*, Nat. Photonics **13**, 714 (2019).
[49] T. Bothwell, D. Kedar, E. Oelker, J. M. Robinson, S. L. Bromley, W. L. Tew, J. Ye, and C. J. Kennedy, Metrologia **56**, 065004 (2019).
[50] W. R. Milner, J. M. Robinson, C. J. Kennedy, T. Bothwell, D. Kedar, D. G. Matei, T. Legero, U. Sterr, F. Riehle, H. Leopardi *et al.*, Phys. Rev. Lett. **123**, 173201 (2019).
[51] E. J. Angstmann, V. A. Dzuba, and V. V. Flambaum, Phys. Rev. A **70**, 014102 (2004).
[52] Y. V. Stadnik and V. V. Flambaum, Phys. Rev. A **93**, 063630 (2016).
[53] See Supplemental Material at http://link.aps.org/supplemental/10.1103/PhysRevLett.125.201302 for More detailed technical information.
[54] J. VanderPlas, A. J. Connolly, Ž. Ivezić, and A. Gray, in *Proceedings of the Conference on Intelligent Data Understanding (CIDU), 2012* (IEEE, New York, 2012), pp. 47–54.
[55] J. T. VanderPlas and Ž. Ivezic, Astrophys. J. **812**, 18 (2015).
[56] K. Van Tilburg, N. Leefer, L. Bougas, and D. Budker, Phys. Rev. Lett. **115**, 011802 (2015).
[57] A. Hees, J. Guéna, M. Abgrall, S. Bize, and P. Wolf, Phys. Rev. Lett. **117**, 061301 (2016).
[58] S. Schlamminger, K.-Y. Choi, T. A. Wagner, J. H. Gundlach, and E. G. Adelberger, Phys. Rev. Lett. **100**, 041101 (2008).
[59] J. Bergé, P. Brax, G. Métris, M. Pernot-Borràs, P. Touboul, and J.-P. Uzan, Phys. Rev. Lett. **120**, 141101 (2018).
[60] G. P. Centers, J. W. Blanchard, J. Conrad, N. L. Figueroa, A. Garcon, A. V. Gramolin, D. F. J. Kimball, M. Lawson, B. Pelssers, J. A. Smiga *et al.*, arXiv:1905.13650.
[61] K. Kuroda and N. Mio, Phys. Rev. Lett. **62**, 1941 (1989).
[62] J. G. Williams, S. G. Turyshev, and D. H. Boggs, Classical Quantum Gravity **29**, 184004 (2012).
[63] A. Arvanitaki, S. Dimopoulos, and K. Van Tilburg, Phys. Rev. Lett. **116**, 031102 (2016).
[64] A. A. Geraci, C. Bradley, D. Gao, J. Weinstein, and A. Derevianko, Phys. Rev. Lett. **123**, 031304 (2019).
[65] M. Bishof, X. Zhang, M. J. Martin, and J. Ye, Phys. Rev. Lett. **111**, 093604 (2013).
[66] H. Y. Carr and E. M. Purcell, Phys. Rev. **94**, 630 (1954).
[67] S. Aharony, N. Akerman, R. Ozeri, G. Perez, I. Savoray, and R. Shaniv, arXiv:1902.02788.
[68] S. Kolkowitz, I. Pikovski, N. Langellier, M. D. Lukin, R. L. Walsworth, and J. Ye, Phys. Rev. D **94**, 124043 (2016).